

Published in final edited form as:

*J Magn Reson Imaging*. 2013 December ; 38(6): . doi:10.1002/jmri.24119.

## QUANTITATIVE MULTI-PARAMETRIC MAGNETIC RESONANCE IMAGING OF OVARIAN CANCER

Jori S. Carter, MD, MS<sup>1</sup>, Joseph S. Koopmeiners, PhD<sup>2</sup>, Jessica E. Kuehn-Hajder, MD<sup>3</sup>, Gregory J. Metzger, PhD<sup>4</sup>, Navneeth Lakkadi, MS<sup>4</sup>, Levi S. Downs Jr., MD, MS<sup>1</sup>, and Patrick J. Bolan, PhD<sup>4</sup>

<sup>1</sup>University of Minnesota, Division of Gynecologic Oncology

<sup>2</sup>University of Minnesota, Division of Biostatistics

<sup>3</sup>University of Minnesota, Department of Radiology

<sup>4</sup>University of Minnesota, Center for Magnetic Resonance Research

### Abstract

**Purpose**—To identify parameters associated with ovarian malignancy using multi-parametric quantitative MRI.

**Materials and Methods**—After IRB approval, women with ovarian masses underwent preoperative imaging with 3 Tesla MRI. DCE-MRI with pharmacokinetic modeling, quantitative T<sub>2</sub> mapping, and diffusion weighted imaging with quantitative mapping of the water diffusion parameters were performed. Ovarian masses had one or more discrete regions of interest, categorized as cystic or solid, and histologically diagnosed as benign or malignant. Mean ROI values were compared between benign and malignant masses using generalized estimating equations. In addition, we compared classification accuracy for the mean ROI value to a combination of histogram characteristics (standard deviation, skewness, and kurtosis) from T<sub>2</sub> map ROIs using logistic regression and ROC curve. Significance level was p=0.05.

**Results**—Several DCE-MRI parameters differentiated solid benign from malignant masses. Toft's rate constant (k<sub>ep</sub>) was significantly higher in malignant masses (p<0.001), as well as quantitative T<sub>2</sub> values (p=0.003), and signal intensity on T<sub>2</sub> weighted imaging (p=0.008). A linear combination of the mean, standard deviation, skewness and kurtosis of T<sub>2</sub> within solid regions (AUC 0.90) provided better classification accuracy than the mean of T<sub>2</sub> alone (AUC 0.81).

**Conclusion**—Quantitative parameters from DCE-MRI and T<sub>2</sub> mapping can differentiate benign from malignant ovarian masses.

### Keywords

magnetic resonance imaging; ovary; neoplasms; methods; investigative techniques

## INTRODUCTION

Ovarian cancer is the leading cause of death from gynecologic cancers among women in the United States (1). Five-year survival rates decrease dramatically from 90% in stage I to 30-40% in stage III and IV patients (2). The near absence of symptoms in early stage and the lack of effective screening tools both contribute to the poor overall survival.

Several diagnostic modalities, including ultrasonography (US), computed tomography (CT), and MRI have been investigated as potential diagnostic and screening tools, and limited data demonstrates sufficient accuracy to predict malignancy either alone or as a part of screening strategy (3-14). Conventional contrast-enhanced MRI has an 84%-93% accuracy to differentiate between malignant and benign lesions (11-13). The interpretation of these images, however, is subjective and may vary depending on the experience of the reader (12). There are a number of objective physical parameters that can be measured with MRI, including relaxation rates, permeability and perfusion parameters derived from dynamic contrast enhanced (DCE) MRI, and diffusion-related parameters. Independently, several of these parameters have been found to be associated with ovarian malignancy: malignant masses have been shown to have shorter T<sub>2</sub> values (14), increased perfusion based on DCE-MRI parameters (15,16), and shorter water apparent diffusion coefficients (ADC) (17) than benign masses. In addition, a combination of DWI parameters, such as T<sub>2</sub> and b<sub>1,000</sub> signal intensity can differentiate benign from malignant ovarian masses (18).

Improved imaging techniques could lead to development of screening modalities, which would increase the likelihood of detecting ovarian cancer at an early stage, and therefore improve survival. In addition, the development of techniques to apply to small volume disease could improve treatment monitoring for ovarian cancer patients.

This study was designed to assess the feasibility of making multiple quantitative parametric measurements within a single study, and to identify which parameters can discriminate between benign and malignant masses. Additionally, we sought to determine whether parameter heterogeneity within a region of interest (ROI), represented by a combination of histogram characteristics, could provide additional information for classifying masses as benign or malignant beyond the mean parameter value. We therefore developed a quantitative multi-parametric MRI protocol, applied it in a pilot study of patients with ovarian masses, and compared our findings to surgical pathology. The aim of this study is to identify quantitative markers that can be used in studies for future development for the detection of early stage ovarian cancer and treatment monitoring.

## MATERIALS AND METHODS

### Patient Characteristics

Approval for this study was obtained from our Institutional Review Board (IRB). Thirtyseven subjects who were scheduled for surgical removal of an ovarian mass suspicious for malignancy by a gynecologic oncologist (based on imaging with either conventional MRI, CT, or US), had no contraindications for MRI were enrolled consecutively, and gave written consent. Subjects with a contraindication to receive gadolinium-DTPA or who had a glomerular filtration rate < 60 mL/min/1.73 m<sup>2</sup> were allowed to participate in the study without the administration of contrast or performance of DCE-MRI. All subjects were evaluated with quantitative MR scanning prior to surgical resection with histological verification.

MRI scans were performed using a 3 Tesla MR scanner (TIM Trio, Siemens, Erlangen, Germany). The images were acquired with patients in the supine position and fitted with standard body matrix and spine array receive coils. Glucagon (0.5 mg intravenous) was given twice, once before scanning and again just prior to the DCE-MRI sequences to minimize small bowel motility in 12 patients (IRB approval of glucagon occurred mid-study). After localizer scans, anatomical imaging was performed using conventional multi-slice T<sub>2</sub>-weighted fast spin-echo images in the axial plane (parameters for all sequences provided in Table 1), and also the coronal and sagittal planes, followed by 3-dimensional T<sub>1</sub>-weighted fat-suppressed axial images covering the pelvis from the pubic symphysis to

the sacral promontory. The anatomical images were then used to identify a target region that included solid regions of the mass if present. Three quantitative imaging series (detailed below) were then analyzed in the axial plane over the target region:  $T_2$  mapping, ADC mapping, and DCE imaging.

### Quantitative Imaging

Reconstructions for all three quantitative methods were performed offline using Matlab (Mathworks, Natick, MA) to produce parameter maps in DICOM format for subsequent analyses. The  $T_2$  mapping acquisition used a two-dimensional multi-echo spin-echo sequence (parameters in Table 1). The multi-echo image set was thresholded to eliminate noise pixels and then fit pixel-by-pixel to a monoexponential decay function to create a  $T_2$  parameter map.

Diffusion weighted images (DWI) were acquired using a single-shot fat suppressed echo-planar imaging sequence with three b-values ( $b=0, 100, 800 \text{ s/mm}^2$ ), three orthogonal diffusion traces, and four averages. All three b-value images were noise-masked, log-transformed, and then fit pixel-by-pixel with a linear model to produce parametric maps of the water ADC. Additional diffusion parameters were calculated using the theory of intravoxel incoherent motion (IVIM) proposed by Le Bihan et al. (19), which aims to separate true diffusion from perfusion effects. Following this method, the  $b=100 \text{ s/mm}^2$  and  $800 \text{ s/mm}^2$  images were used to calculate maps of the true diffusion coefficient IVIM-D, and subsequently the perfusion fraction IVIM- $F_p$ .

DCE acquisitions consisted of a series of forty 3D fat-suppressed gradient echo volumes, with a temporal resolution of 8.45 s/frame. Intravenous contrast injection (0.1 mmol/kg, 3 mL/s, 20 mL saline flush) was started after completion of four complete frames. The dynamic time series was noise masked and analyzed pixel-by-pixel using three previously established techniques. First, the normalized signal intensity was fit to a sigmoid function, as previously shown in ovarian cancer by Thomassin-Naggara et al. (16), to estimate the enhancement amplitude (EA), time of half rising  $T_{h_1}$ , and maximal slope (MS) of the sigmoid curve. Secondly, the signal intensity was converted to a concentration by assuming a fixed pre-contrast  $T_1$  value of 1500 ms, as suggested by Guo et al. (20). The first 60 seconds after contrast injection were integrated to calculate the initial area under the Gadolinium concentration curve (IAUC60). Finally, assuming a fixed, population averaged arterial input function (21), the Gd concentration curve was fit to the extended Tofts' two-compartment model (22) to estimate the transfer constant  $K_{trans}$ , the rate constant  $k_{ep}$ , and the relative volume of the extravascular extracellular space,  $v_e$ .

In addition to these eleven quantitative parameters, normalized values for IAUC60, EA, and the axial  $T_2$ -weighted anatomical image were produced by dividing by the mean value of an ROI placed adjacent skeletal muscle (piriformis when possible, gluteus maximus otherwise) to normalize for variation in cardiac output and system calibrations between subjects. The quantitative parameters assessed are summarized in Table 2.

### Analysis

A blinded radiologist (6 years of experience in pelvic MRI) was presented with the anatomical images on an Osirix workstation (23) and asked to prescribe two-dimensional polygonal ROIs on a representative slice for each distinct region larger than 2 cm within all ovarian masses, whether single, bilateral, or multiple, within each subject. Each ROI was then subjectively identified as predominantly cystic or solid based on morphology and intensity in the  $T_2$ -weighted anatomical images. ROIs were copied to the parametric maps, with minor manual adjustments as needed to adjust for motion between the acquisitions and

distortion on the DWI images. Histograms were generated for each ROI on all intersecting parametric maps and summary statistics (mean, standard deviation, skewness, and kurtosis) were recorded. Noise-masked pixels were excluded from the analysis.

The primary analyses compared the mean value of each parameter in each ROI to histology outcome using generalized estimating equations with exchangeable working correlation structure to account for the potential correlation between multiple ROIs from the same subject. Secondary analyses were performed by considering the solid and cystic ROIs separately. Bonferroni corrections for multiple comparisons were not applied in these exploratory analyses due to the small numbers in the study. For the histogram analysis, we compared the classification accuracy of the ROI mean value alone versus a linear combination of histogram characteristics (mean, standard deviation, skewness, and kurtosis) from each ROI. Linear model coefficients were estimated using logistic regression and the linear combination of the four parameters represents the fitted value for each ROI. The classification accuracy of our model was evaluated using the receiver-operating characteristic (ROC) curve, which was estimated using leave-one-out cross validation (CV) to correct for overfitting. We used the area under the ROC curve (AUC) to compare our fitted model to the classification accuracy for the mean ROI value alone. Confidence intervals for the AUC were estimated by bootstrap. All statistical calculations were performed with the R statistical software environment (24) and used a 0.05 significance level.

## RESULTS

A total of 37 women with adnexal masses gave informed consent and were prospectively and consecutively enrolled in the study. All subjects were scheduled for surgical removal of at least one ovary. One subject was excluded from the analysis because her mass was not ovarian, and two were excluded because they had low malignant potential/borderline ovarian tumors. Thirty-four women were included in the analysis, 12 with malignant ovarian masses and 22 benign. Mean age was 53.6 years (range 34–87). The histologic diagnoses of the 37 women enrolled are detailed in Table 3. Several of these subjects did not have the full set of parametric data included in the analyses: ten subjects were unable to receive gadolinium-DTPA due to contraindications and therefore had no contrast-related parametric maps (3 malignant, 7 benign); three subjects had diffusion-weighted imaging that was judged unacceptable due to artifacts and therefore had no diffusion-related parametric maps (1 malignant, 2 benign). All 34 subjects had acceptable T<sub>2</sub>-weighted imaging and T<sub>2</sub> maps. The full anatomic and quantitative imaging protocol was completed in an average of 52 minutes (range 42–64).

Using the anatomical images, the radiologist prescribed a total of 109 lesion ROIs in the 34 subjects, with either single, bilateral, or multiple ovarian masses. Cystic ROIs were more common: the 22 benign cases included 8 solid ROIs and 41 cystic ROIs, whereas the 12 malignant cases included 20 solid and 40 cystic ROIs. The ROIs were then transferred to all overlapping parametric maps for each of the 15 parameters in Table 2. Note that the parametric acquisitions had reduced coverage in the slice direction compared to the anatomical images, and therefore not all ROIs were representable in all parametric maps. A total of 1696 combinations of ROI and parametric map were considered for subsequent analyses. Examples of ROIs on anatomical and parametric images are given for a benign case (Figure 1) and a malignant case (Figure 2).

The first analysis assessed the mean parametric value within each ROI to identify which MRI parameters were associated with malignancy. Both solid and cystic ROIs were included in this analysis. The results are summarized in Table 4. Most of the DCE parameters had

significantly higher mean values in malignant masses compared to benign masses, including IAUC, IAUC-ref,  $K_{trans}$ ,  $k_{ep}$ , sigmoid EA, and sigmoid EA-ref ( $p < .001$  in all cases). Additionally, the mean values from the  $T_2$  maps were significantly lower in malignant masses compared in benign masses ( $p = 0.028$ ). There were no statistically significant differences with the diffusion-related parameters.

To correct for the potentially confounding effect of cystic versus solid ROIs, the analysis was repeated separately for solid ROIs and cystic ROIs. The results from analyzing only the solid ROIs are summarized in Table 5. Several DCE parameters were significantly different between benign and malignant solid regions, including IAUC-ref,  $k_{ep}$ , sigmoid EA-ref, and sigmoid  $T_h$  ( $p = 0.028$ ,  $< 0.001$ ,  $0.025$ ,  $0.019$ , respectively). With the cyst ROIs removed, the  $T_2$  values are higher in malignant solid regions, with significant differences in the  $T_2$  map, the  $T_2$  weighted image signal intensity ( $T_2$ -w) and the normalized signal intensity ( $T_2$ w-ref) ( $p = 0.003$ ,  $0.008$ ,  $< 0.001$ , respectively). No difference was found in ADC or D, but the perfusion fraction  $F_p$  was significantly lower in malignant solid regions ( $p = 0.043$ ).

Even though cystic ROIs generally do not enhance, the predominantly cystic ROIs were analyzed with DCE so that our methods were consistent. Several DCE parameters had higher mean values in malignant cystic regions compared to benign cystic regions, including IAUC ( $p < 0.001$ ), IAUC-ref ( $p = 0.013$ ),  $K_{trans}$  ( $p = 0.001$ ), sigmoid EA ( $p = 0.002$ ), and sigmoid EA-ref ( $p = 0.001$ ) (data not shown). No significant differences were found with the  $T_2$  parameters or the diffusion-related parameters.

Finally, we compared the classification accuracy of the ROI mean value alone versus a combination of histogram characteristics from each ROI. For this analysis, the data were filtered to select only those ROI/parameter map combinations with reliable distribution metrics: ROI/parameter map combinations that had fewer than 100 pixels after noise thresholding, or less than 33% pixels included after noise thresholding were removed from the analysis. After this filtering, the remaining data contained too few ROIs to adequately assess the DWI and DCE parameters, so the histogram analysis focused solely on the  $T_2$ -related parameters. Figure 3 gives examples of ROIs on  $T_2$  maps and their associated histogram characteristics for benign and malignant cases.

Table 6 presents AUC for the mean  $T_2$  imaging parameters and for a linear combination of the mean, standard deviation, skewness and kurtosis for each  $T_2$  imaging parameter. The CV adjusted AUC for a linear combination of the four histogram characteristics for  $T_2$  map increased to 0.90 (95% CI: 0.83, 1.00), compared to an AUC of 0.81 (0.56, 1.00) for the mean alone. This suggests there is additional information for predicting histology outcome beyond the mean of the  $T_2$  map. In contrast, the AUC for  $T_2$ w and  $T_2$ w-ref actually decreased when adding additional histogram characteristics to the model, suggesting that the additional data are simply adding noise to the model and are not associated with benign or malignant masses.

## DISCUSSION

In conclusion, we have demonstrated the feasibility of performing multi-parametric, quantitative MRI for the characterization of ovarian masses, and found several parameters based on DCE-MRI, diffusion imaging, and  $T_2$  relaxometry that were significantly associated with malignancy. The most objective findings were based on the first analysis, which used only ROI means and included all ROIs without subjectively distinguishing between predominantly cystic and solid ROIs. For this analysis, both DCE-MRI and  $T_2$ -based acquisitions produced significant parameters, while diffusion imaging did not. These findings, however, were confounded by composition of the ROIs: predominantly cystic



regions generally have longer  $T_2$  values and do not enhance, and purely cystic masses are most always benign.

The second analysis, which used only ROI means and only in predominantly solid ROIs, is more relevant to the diagnostic setting where the radiologist is concerned about suspicious solid regions. In this analysis, several parametrics from DCE-MRI,  $T_2$  imaging, and diffusion imaging were associated with malignancy. The DCE-MRI findings were expected and consistent with previous literature (16), as malignant ovarian masses are known to have increased vascularity. Significant associations were found in parameters derived from each of the three distinct DCE-MRI analysis approaches (area under curve, sigmoid fitting, and pharmacokinetic modeling), suggesting that the diagnostic information is inherent in the data and robust with respect to analysis method. Our finding that quantitative  $T_2$  mapping was associated with ovarian malignancy has not been previously reported. This is, however, consistent with the practice of using hypo- and hyper-intensity on  $T_2$ -weighted imaging as a diagnostic feature (14), but with the added advantage of being assessed quantitatively. The diffusion parameters performed more poorly than expected, with no association between ADC in either the solid-only or the solid+cyst analysis. This finding was consistent with one prior study (18,25), but inconsistent with several previous reports using 1.5T MRI (17,26-29). This may be attributable to our sequence optimization; we scanned with a high resolution ( $192 \times 192$  matrix) while using a large acceleration factor ( $R=3$ ) to keep the echo train short, and this approach may have led to insufficient signal-to-noise ratio (SNR). Further work is warranted to optimize the diffusion-weighted imaging methods for high-resolution and good SNR at 3T. We did find that the perfusion fraction  $F_p$ , as estimated by the IVIM technique, was lower in malignant solid regions than in benign solid regions. This finding should be interpreted cautiously, as it is inconsistent with the increased vascularity shown in our DCE-MRI findings. The 3 b-value technique we used to calculate  $F_p$  was consistent with the originally reported IVIM method (19), but the  $F_p$  maps had generally low signal-to-noise, and more b-values should be used in future studies to assess IVIM parameters.

The histogram analysis illustrates that other characteristics of the  $T_2$  map distribution beyond the mean provide additional information for discriminating between benign and malignant regions. One explanation may be that malignant masses are typically heterogeneous with a combination of cystic and solid elements, while the majority of benign masses are cystic and homogenous. Even when focusing on only the solid components of both malignant and cystic masses, malignant solid masses have small necrotic regions (12), whereas the benign solids generally appeared to be more fibrous and uniform. Considering all three analyses, the quantitative  $T_2$  mapping was stronger than  $T_2$ -weighted imaging signal intensity, with or without normalization by a reference ROI. This  $T_2$  mapping has the advantage of removing receive coil sensitivity,  $T_1$  weighting, and proton density effects, and is therefore are more direct reflection of the underlying tissue relaxation rate.

Our study has several limitations. First, for the number of parameters investigated and the multiple comparisons performed, the number of subjects enrolled was small. This may decrease the strength of the associations that were seen in this exploratory study, particularly for those in the smallest cohorts. Second, we did not compare the performance of the metrics with conventional interpretation of the anatomic images, as the study was designed to identify potential diagnostic biomarkers rather than assess diagnostic performance. Third, due to variations in spatial coverage between the imaging methods as well as the small study size, we did not have sufficient data to assess the feasibility of using combined parameters (e.g.,  $T_2$  and ADC together) in a diagnostic model. Fourth, borderline ovarian tumors comprised 5.4% of patients with ovarian masses who were enrolled in our study ( $n=2$ ), and they were excluded from the analysis because of the small number. The inclusion of larger

numbers of borderline tumors in future trials could be important because there may be distinct differences between the quantitative MRI values in borderline ROIs compared to benign and malignant ROIs. Borderline ovarian tumors are treated surgically, so it would be valuable to differentiate them from benign masses.

In conclusion, the development of innovative, quantitative MRI techniques for potential screening and treatment monitoring applications motivates our investigation into quantitative MRI. Utilizing our exploratory data in future studies could contribute to the development of a non-contrast ovarian MRI exam using quantitative T<sub>2</sub> mapping along with conventional image interpretation; this would reduce scan times and cost, and could be useful for potential future studies of new screening modalities. Additionally, based on our exploratory findings, future studies could evaluate the accuracy of a contrast-enhanced MRI study using T<sub>2</sub> mapping methods for the characterization ovarian masses.

## Acknowledgments

The authors wish to thank Diane Hutter R.N. for managing and preparing the patients, and to Siemens for provide works-in-progress software packages.

**Funding:** NCRR P41 RR008079, P41 EB015894, NIBIB P41 EB015894, NIH T32 CA132715, The Randy Shaver Foundation, and the University of Minnesota Academic Health Center Faculty Seed Grant

## REFERENCES

1. American, Cancer Society. Cancer Facts and Figures 2009. American Cancer Society; Atlanta: 2009.
2. Munkarah A, Chatterjee M, Tainsky M. Update on ovarian cancer screening. *Curr Opin Obstet Gynecol.* 2007; 19:22–26. [PubMed: 17218847]
3. Menon U, Gentry-Maharaj A, Hallett R, et al. Sensitivity and specificity of multimodal and ultrasound screening for ovarian cancer, and stage distribution of detected cancers: results of the prevalence screen of the UK Collaborative Trial of Ovarian Cancer Screening (UKCTOCS). *Lancet Oncol.* 2009; 10:327–340. [PubMed: 19282241]
4. Buy JN, Ghossain MA, Hugol D, et al. Characterization of adnexal masses: combination of color Doppler and conventional sonography compared with spectral Doppler analysis alone and conventional sonography alone. *AJR.* 1996; 166:385–393. [PubMed: 8553953]
5. Stein SM, Laifer-Narin S, Johnson MB, et al. Differentiation of benign and malignant adnexal masses: relative value of gray-scale, color Doppler, and spectral Doppler sonography. *AJR.* 1995; 164:381–386. [PubMed: 7839975]
6. Levine D, Feldstein VA, Babcock CJ, Filly RA. Sonography of ovarian masses: poor sensitivity of resistive index for identifying malignant lesions. *AJR.* 1994; 162:1355–1359. [PubMed: 8191998]
7. Rehn M, Lohmann K, Rempen A. Transvaginal ultrasonography of pelvic masses: evaluation of B-mode technique and Doppler ultrasonography. *Am J Obstet Gynecol.* 1996; 175:97–104. [PubMed: 8694082]
8. Buys SS, Partridge E, Greene MH, et al. PLCO Project Team. Ovarian cancer screening in the Prostate, Lung, Colorectal and Ovarian (PLCO) cancer screening trial; findings from the initial screen of a randomized trial. *Am J Obstet Gynecol.* 2005; 193:1630–1639. [PubMed: 16260202]
9. Buys SS, Partridge E, Black A, et al. for the PLCO Project Team. Effect of screening on ovarian cancer mortality: the prostate, lung, colorectal and ovarian (PLCO) cancer screening randomized controlled trial. *JAMA.* 2011; 305:2295–2303. [PubMed: 21642681]
10. van Nagell JR, DePriest PD, Ueland FR, et al. Ovarian cancer screening with annual transvaginal sonography: findings of 25,000 women screened. *Cancer.* 2007; 109:1887–1896. [PubMed: 17373668]
11. Booth SJ, Turnbull LW, Poole DR, Richmond I. The accurate staging of cancer using 3T magnetic resonance imaging – a realistic option. *BJOG.* 2008; 115:894–901. [PubMed: 18485169]

12. Hricak H, Chen M, Coakley FV, et al. Complex adnexal masses: detection and characterization with MR imaging - multivariate analysis. *Radiology*. 2000; 214:39–46. [PubMed: 10644099]
13. Sohaib SA, Sahdev A, Van Trappen P, Jacobs JJ, Reznick RH. Characterization of adnexal mass lesions on MR imaging. *Am J Roentgenol*. 2003; 180:1297–1304. [PubMed: 12704041]
14. Thomassin-Naggara I, Toussaint I, Perrot N, et al. Characterization of complex adnexal masses: value of adding perfusion- and diffusion-weighted MR imaging to conventional MR imaging. *Radiology*. 2011; 258:793–803. [PubMed: 21193596]
15. Thomassin-Naggara I, Darai E, Cuenod CA, Rouzier R, Callard P, Bazot M. Dynamic contrast-enhanced magnetic resonance imaging: a useful tool for characterizing ovarian epithelial tumors. *J Magn Reson Imaging*. 2008; 28:111–120. [PubMed: 18581400]
16. Thomassin-Naggara I, Bazot M, Darai E, Callard P, Thomassin J, Cuenod CA. Epithelial ovarian tumors: value of dynamic contrast-enhanced MR imaging and correlation with tumor angiogenesis. *Radiology*. 2008; 248:148–159. [PubMed: 18458244]
17. Moteki T, Ishizaka H. Diffusion-weighted EPI of cystic ovarian lesions: evaluation of cystic contents using apparent diffusion coefficients. *J Magn Reson Imaging*. 2000; 12:1014–1019. [PubMed: 11105044]
18. Thomassin-Naggara I, Darai E, Cuenod CA, et al. Contribution of diffusion-weighted MR imaging for predicting benignity of complex adnexal masses. *Eur Radiol*. 2009; 19:1544–1552. [PubMed: 19214523]
19. Le Bihan D, Breton E, Lallemand D, Aubin ML, Vignaud J, Laval-Jeantet M. Separation of diffusion and perfusion in intravoxel incoherent motion MR imaging. *Radiology*. 1998; 168:497–505. [PubMed: 3393671]
20. Guo JY, Reddick WE, Rosen MA, Song HK. Dynamic contrast-enhanced magnetic resonance imaging parameters independent of baseline T10 values. *Magn Reson Imaging*. 2009; 27:1208–1215. [PubMed: 19559556]
21. Parker GJ, Roberts C, Macdonald A, et al. Experimentally-derived functional form for a population-averaged high-temporal-resolution arterial input function for dynamic contrast-enhanced MRI. *Magn Reson Med*. 2006; 56:993–1000. [PubMed: 17036301]
22. Tofts PS, Brix G, Buckley DL, et al. Estimating kinetic parameters from dynamic contrast-enhanced T1-weighted MRI of a diffusible tracer: standardized quantities and symbols. *J Magn Reson Imaging*. 1999; 10:223–232. [PubMed: 10508281]
23. OsiriX Imaging Software. [March 30, 2012] Advanced Open-Source PACS Workstation DICOM Viewer. OsiriX Website. <http://www.osirix-viewer.com>.
24. R Project. [March 30, 2012] R Version 2.14.2012-03-14. R Project Website. <http://cran.r-project.org/doc/FAQ/R-FAQ.html>. ISBN 3-900051-08-9.
25. Fujii S, Kakite S, Nishihara K, et al. Diagnostic accuracy of diffusion-weighted imaging in differentiating benign from malignant ovarian lesions. *J Magn Reson Imaging*. 2008; 28:1149–1156. [PubMed: 18972356]
26. Katayama M, Masui T, Kobayashi S, et al. Diffusion-weighted echo planar imaging of ovarian tumors: is it useful to measure apparent diffusion coefficients? *J Comp Assist Tomogr*. 2002; 26:250–256.
27. Kyriazi S, Collins DJ, Messiou C, et al. Metastatic ovarian and peritoneal cancer: assessing chemotherapy response with diffusion-weighted MR imaging- value of histogram analysis of apparent diffusion coefficients. *Radiology*. 2011; 261:182–192. [PubMed: 21828186]
28. Nakayama T, Yoshimitsu K, Irie H, et al. Diffusion-weighted echo-planar MR imaging and ADC mapping in the differential diagnosis of ovarian cystic masses: usefulness of detecting keratinoid substances in mature cystic teratomas. *J Magn Reson Imaging*. 2005; 22:271–278. [PubMed: 16028258]
29. Namimoto T, Awai K, Nakaura T, Yanaga Y, Hirai T, Yamashita Y. Role of diffusion-weighted imaging in the diagnosis of gynecological diseases. *Eur Radiol*. 2009; 19:745–760. [PubMed: 18839179]



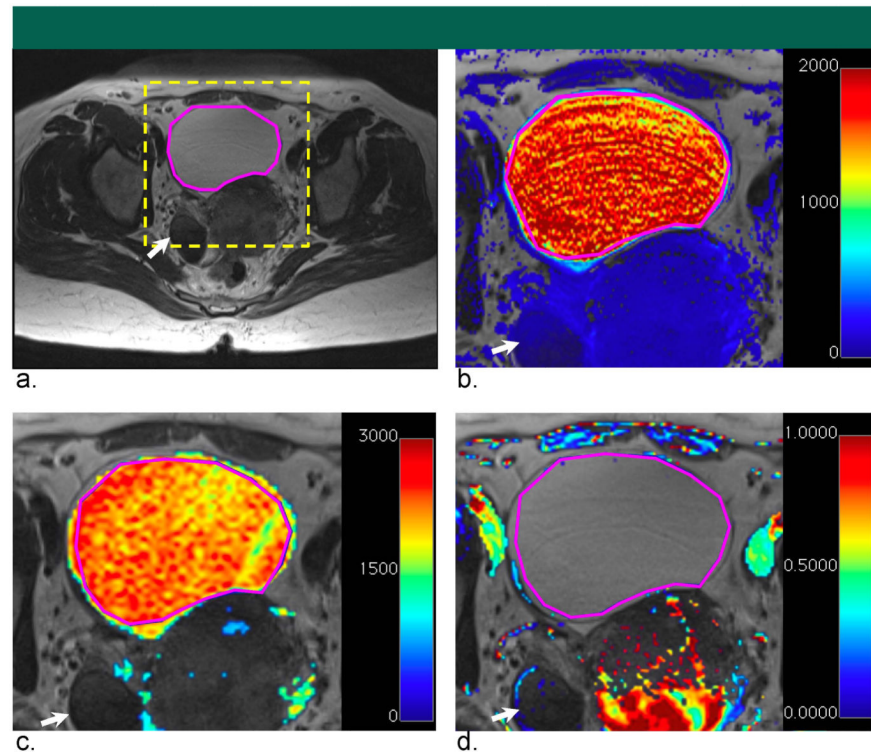


**Figure 1.**

Example of multiparametric images for a benign serous cystadenoma (subject #37). (a) Anatomical T<sub>2</sub>-weighted image with ROI on the large cyst. (b) T<sub>2</sub> map (ms), (c) ADC map (10<sup>-6</sup> mm<sup>2</sup>/s), and (d) Toft's model k<sub>ep</sub> map (min<sup>-1</sup>) overlaid on the anatomical image with ROI indicated. The quantitative maps indicate the cystic fluid has a long T<sub>2</sub> (mean 1877 ms), high ADC (mean  $2.7 \times 10^{-3}$  mm<sup>2</sup>/s), and no contrast enhancement. Also visible is a hemorrhagic corpus luteum (white arrow), whose ROI was drawn on an adjacent slice, that exhibits short T<sub>2</sub>, negligible enhancement, and low SNR on the diffusion images.

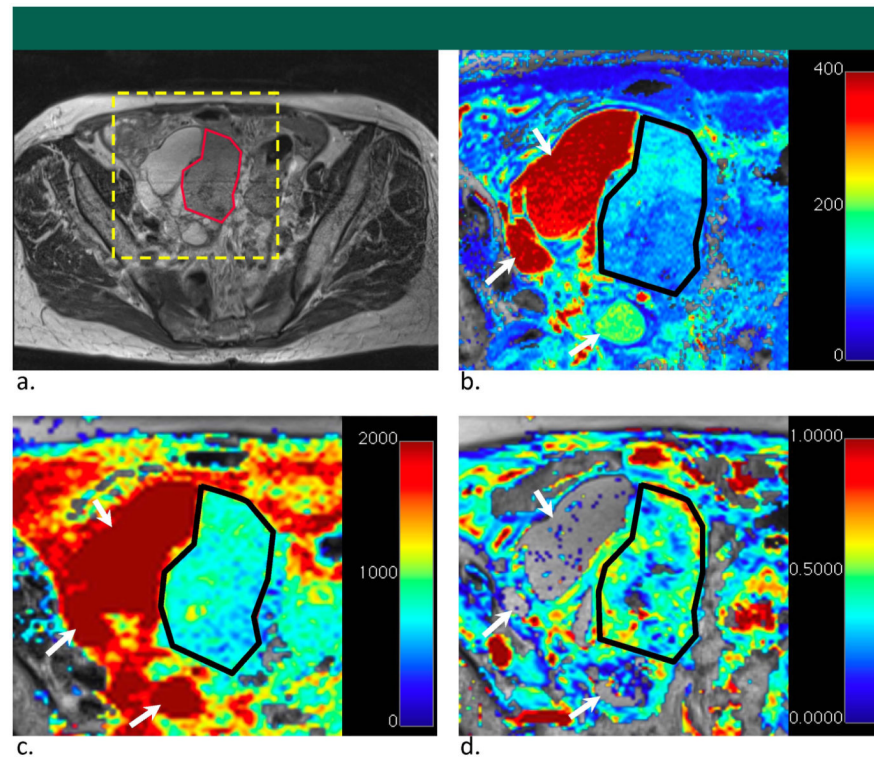


**Figure 2.**

Example of multiparametric images for a stage IIIC serous adenocarcinoma of the ovary (subject #21). (a) Anatomical T<sub>2</sub>-weighted image with ROI on the largest solid component of the mass. (b) T<sub>2</sub> map (ms), (c) ADC map ( $10^{-6} \text{ mm}^2/\text{s}$ ), and (d) Toft's model  $k_{ep}$  map ( $\text{min}^{-1}$ ) overlaid on the anatomical image with ROI indicated. The maps show this solid region has a relatively short T<sub>2</sub> (118.5 ms) and low ADC (mean  $0.86 \times 10^{-3} \text{ mm}^2/\text{s}$ ), suggestive of high cellularity. The high  $k_{ep}$  value (mean  $0.45 \text{ min}^{-1}$ ) indicates the mass is mostly well-vascularized with regions of poor perfusion. Cystic regions of the same complex mass (white arrows) exhibit variable T<sub>2</sub> values, high ADC, and low enhancement.

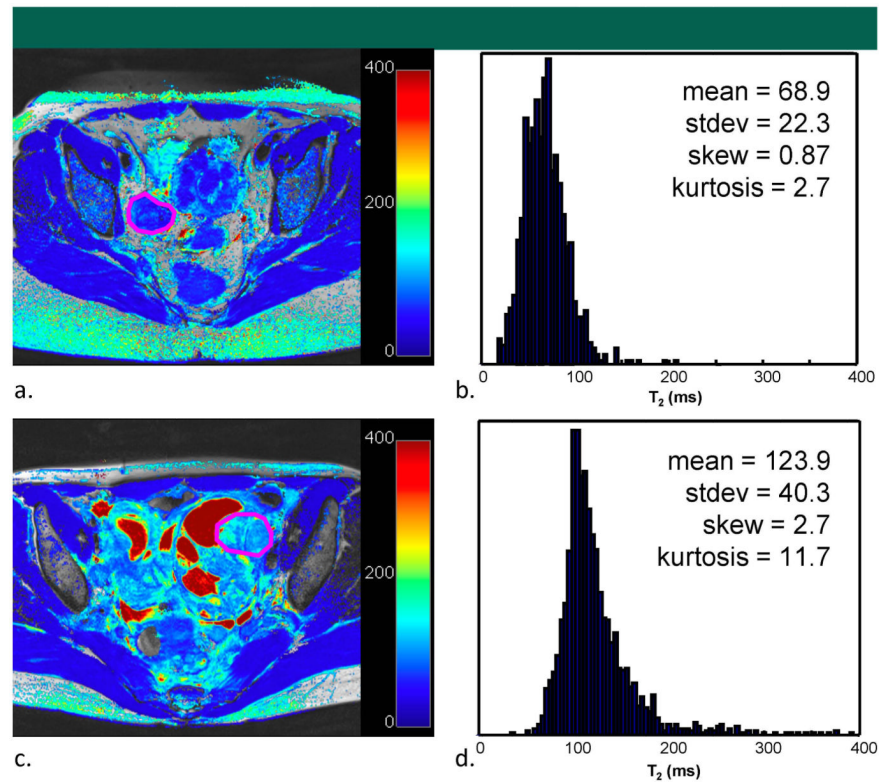


**Figure 3.**

Illustration of the distribution of  $T_2$  values within solid ROIs. Top row shows the (a)  $T_2$  map with ROI in a solid region of a benign fibrothecoma (subject #35), and (b) histogram of  $T_2$  values from the ROI. Bottom row shows a (c)  $T_2$  map and ROI in a solid region of a malignant serous adenocarcinoma (subject #33) and (d) associated histogram. In this comparison the benign solid ROI had a shorter mean  $T_2$  value and a more uniform distribution of  $T_2$  values (b) compared to the longer  $T_2$  values and more skewed distribution for the malignant solid ROI (d).

Table 1

Parameters of MR sequences.

	T <sub>2</sub> -weighted axial	T <sub>2</sub> -weighted coronal & sagittal	T <sub>1</sub> -weighted axial	T <sub>2</sub> map	DWI	DCE
TR (ms)	3350	7380	4.0	3000	4000	3.5
TE (ms)	95	104	1.4	13-324 in 24 steps	53	1.2
Echo-train length	29	29	-	24	64	-
Flip angle (°)	90/120	90/120	10	90/180	90/180	8
Section thickness (mm)	4.0	4.0	3.0	3.0	4.0	4.0
# Sections	36	30	52	7	24	22
Readout Field of view (mm)	280-420	280-420	250-400	240-380	300-400	240-320
Phase encode Field (% of readout)	75%	75%	75%	75%	100%	100%
Matrix	384×384	320×240	384×384	384×258	192×192	192×164
Parallel Reduction	2	1 (cor)	none	none	3	2
Factor		none (sag)				
Acquisition time (s)	117	120	41	296	132	8.45

**Table 2**

Description of the multiple MRI parameters.

Category	Parameter	Description	Units
DWI	ADC	Apparent diffusion coefficient	mm <sup>2</sup> /s
	IVIM-D	IVIM-derived diffusion coefficient	mm <sup>2</sup> /s
	IVIM-fp	IVIM-derived perfusion fraction	(ratio)
DCE	IAUC60	Initial area under the Gd concentration curve, 60 seconds	mM*s
	IAUC60-ref	IAUC60 normalized by muscle reference	(ratio)
DCE Tofts	Ktrans	Tofts' volume transfer constant	min <sup>-1</sup>
	k <sub>ep</sub>	Tofts' rate constant	min <sup>-1</sup>
	Ve	Tofts' relative volume of EES per unit volume of tissue	(ratio)
DCE sigmoid	EA	Sigmoid enhancement amplitude	a.u.
	EA-ref	Sigmoid EA normalized by muscle reference	(ratio)
	Th	Sigmoid time of half-rising	s
	MS	Sigmoid maximum slope	a.u.
T <sub>2</sub>	T <sub>2w</sub>	Axial T2w anatomical image signal intensity	a.u.
	T <sub>2w</sub> -ref	Axial T2w anatomical image signal intensity normalized by muscle reference	(ratio)
	T <sub>2</sub>	Transverse relaxation time constant	ms



Table 3

Characteristics and histology of all women enrolled.

Patient No.	Age	Largest dimension of mass, encompassing all ROIs (cm)	# Cystic ROIs	# Solid ROIs	Diagnosis	Histologic subtype
1	41	9	1	1	Benign	Endometriosis
2	62	27.3	1	1	Malignant, stage IA	Clear cell carcinoma
3	41	7.9	5	0	Benign	Endometriosis
4	43	11.6	3	0	Benign	Mucinous cystadenoma
5	63	4.3	0	2	Benign	Fibroma
6	37	14.1	4	0	Benign	Adenofibroma and endometriosis
7	54	24.3	3	0	Benign	Hemorrhagic cyst
8	62	5.9	0	1	Benign	Brenner tumor
9	39	4.5	1	0	Benign	Endometriosis
10	50	10.9	0	1	Malignant, stage II	Fibrosarcoma
11	49	5.1	1	0	Benign	Adenofibroma
12	58	20.9	1	0	Benign	Mucinous cystadenoma and
13	39	18.6	1	0	Benign	Mature teratoma
14	52	18.8	3	1	Benign	Serous cystadenoma
15*	44	6.6	3	0	Borderline, Stage IA	Serous cystadenoma
16	68	9.7	5	2	Malignant, stage IIIC	Serous adenocarcinoma
17	75	18.7	4	0	Malignant, stage IA	Mucinous adenocarcinoma
18	51	11.3	5	1	Malignant, stage IV	Serous adenocarcinoma
19	59	4.1	1	0	Benign	Histologically normal ovarian tissue
20	67	3.2	0	1	Benign	Serous cystadenoma
21	75	9.1	2	1	Malignant, stage IIIC	Serous adenocarcinoma
22	69	10.3	1	3	Malignant, stage IIIC	Serous adenocarcinoma
23	45	20.5	4	0	Benign	Mucinous cystadenoma
24	46	16	3	3	Malignant, stage IA	Endometrioid adenocarcinoma
25	49	24.4	5	3	Malignant, stage IIIC	Serous adenocarcinoma
26	35	3.8	2	1	Benign	Serous cystadenoma
27	87	16.7	3	1	Malignant, stage IIIC	Serous adenocarcinoma
28	52	9.1	1	0	Benign	Serous cystadenoma

Patient No.	Age	Largest dimension of mass, encompassing all ROIs (cm)	# Cystic ROIs	# Solid ROIs	Diagnosis	Histologic subtype
29*	74	10.1	2	2	Borderline, stage IC	Endometrioid adenocarcinoma
30*	48	10.4	2	1	Borderline	Uterine smooth muscle tumor of
31	45	17.3	5	0	Benign	Mucinous cystadenoma
32	46	28.2	6	2	Malignant, stage IIC	Serous adenocarcinoma
33	49	14.3	5	2	Malignant, stage IV	Serous adenocarcinoma
34	34	4.3	2	0	Benign	Hemorrhagic cyst
35	64	4.3	0	1	Benign	Fibrothecoma
36	70	2.9	1	0	Benign	Epithelial inclusion cyst of the ovary
37	49	8.7	2	0	Benign	Serous cystadenoma

\* Subjects 15, 30, and 29 were excluded from the study for non-ovarian pathology or borderline tumors.

Table 4

The mean values in solid and cystic ROIs combined.

Parameter	Benign			Malignant			p-value
	N subject	N ROI	Mean value	N subject	N ROI	Mean value	
DWI							
ADC (mm <sup>2</sup> /s)	20	40	1924.88	11	50	1747.79	0.162
D (mm <sup>2</sup> /s)	19	37	1872.46	11	50	1700.96	0.224
F <sub>p</sub>	19	37	8.35	11	50	9.01	0.741
DCE							
IAUC (mM <sup>*</sup> s)	14	27	0.90	9	40	3.35	<0.001 <sup>*</sup>
IAUC-ref	13	26	1.04	9	40	3.69	<0.001 <sup>*</sup>
K <sub>trans</sub> (min <sup>-1</sup> )	15	33	0.01	9	40	0.05	<0.001 <sup>*</sup>
k <sub>ep</sub> (min <sup>-1</sup> )	15	33	0.23	9	40	0.40	<0.001 <sup>*</sup>
v <sub>e</sub>	15	33	0.28	9	40	0.27	0.805
sigmoidEA (a.u)	14	27	0.21	9	40	0.54	<0.001 <sup>*</sup>
sigmoidEA-ref	13	27	0.80	9	40	2.39	<0.001 <sup>*</sup>
sigmoidTh (s)	15	33	25.75	9	40	28.29	0.432
sigmoidMS×10 <sup>3</sup> (a.u.)	15	33	142.64	9	40	107.91	0.199
T <sub>2</sub>							
T <sub>2</sub> w (a.u.)	22	48	951.45	12	59	844.45	0.211
T <sub>2</sub> w-ref	22	48	4.11	12	59	3.44	0.080
T <sub>2</sub> map (s)	22	47	452.85	11	43	271.38	0.028 <sup>*</sup>

<sup>\*</sup> Denotes significance at the p=0.05 level

**Table 5**

The mean values of solid ROIs in benign and malignant ovarian tumors.

Parameter	Benign			Malignant			p-value
	N subject	N ROI	Mean Value	N subject	N ROI	Mean Value	
DWI							
ADC (mm <sup>2</sup> /s)	6	6	1249.35	10	16	1143.44	0.609
D (mm <sup>2</sup> /s)	6	6	1187.09	10	16	1094.90	0.668
F <sub>p</sub>	6	6	11.27	10	16	8.95	0.043 <sup>*</sup>
DCE							
IAUC (mM <sup>*</sup> s)	4	4	3.79	9	16	6.89	0.066
IAUC-ref	4	4	3.67	9	16	7.47	0.028 <sup>*</sup>
K <sub>trans</sub> (min <sup>-1</sup> )	4	4	0.06	9	16	0.10	0.069
k <sub>ep</sub> (min <sup>-1</sup> )	4	4	0.27	9	16	0.47	<0.001 <sup>*</sup>
v <sub>e</sub>	4	4	0.30	9	16	0.26	0.370
sigmoidEA (a.u)	4	4	0.69	9	16	0.89	0.239
sigmoidEA-ref	4	4	2.43	9	16	3.83	0.025 <sup>*</sup>
sigmoidTh (s)	4	4	38.06	9	16	26.18	0.019 <sup>*</sup>
sigmoidMS×10 <sup>3</sup> (a.u.)	4	4	48.83	9	16	91.31	0.129
T <sub>2</sub>							
T <sub>2</sub> w (a.u.)	7	8	426.61	11	19	621.33	0.008 <sup>*</sup>
T <sub>2</sub> w-ref	7	8	1.704	11	19	2.58	<0.001 <sup>*</sup>
T <sub>2</sub> map (s)	7	8	81.92	10	18	128.90	0.003 <sup>*</sup>

\* Denotes significance at the p=0.05 level

Table 6

AUC for T<sub>2</sub> imaging weighted imaging and kep in solid ROIs.

Parameter	Benign		Malignant		AUC of Mean Only		Cross-Validation Adjusted AUC of Combined Values <sup>*</sup>		
	N	subject	N	subject	N	AUC	95% CI	AUC	95% CI
T <sub>2</sub> w	7		8	11	19	0.83	(0.64, 0.99)	0.68	(0.45, 1)
T <sub>2</sub> w-ref	7		8	11	19	0.85	(0.67, 0.97)	0.78	(0.63, 1)
T <sub>2</sub> map	7		7	10	18	0.81	(0.56, 1)	0.90	(0.83, 1)
kep	4		4	9	16	0.97	(0.85, 1)	**	**

\* A linear model of the mean, standard deviation, skewness and kurtosis

\*\* There were too few ROIs to meaningfully evaluate the DCE parameters by the cross-validated linear model of the combination of the mean, standard deviation, skewness and kurtosis.